Computation & theory

Unraveling the enhanced stability and strength of Al Σ9 (221)[1̄10] symmetric tilt grain boundary with Mg segregation

Ning Ma[1], Dongdong Zhao[1,*] , Chunsheng Shi[1], Chunnian He[1,2,3], Enzuo Liu[1], Junwei Sha[1], Yanjun Li[4,*], and Naiqin Zhao[1,2]

[1] School of Materials Science and Engineering and Tianjin Key Laboratory of Composites and Functional Materials, Tianjin University, Tianjin 300350, China

[2] Key Laboratory of Advanced Ceramics and Machining Technology, Ministry of Education, Tianjin University, Tianjin 300072, China

[3] Joint School of National University of Singapore and Tianjin University, International Campus of Tianjin University, Binhai New City, Fuzhou 350207, China

[4] Department of Materials Science and Engineering, Norwegian University of Science and Technology (NTNU), 7491 Trondheim, Norway

ABSTRACT

The marked Mg segregation at grain boundaries (GBs) in nanocrystalline Al alloys usually contributes additional GB segregation strengthening. To gain a further understanding of this phenomenon, molecular dynamics simulations were conducted to reveal the Mg segregation behavior at Al Σ9 (221)[1̄10] symmetric tilt grain boundary (STGB) and its effects on the GB stability and strength. Results reveal that Mg dopants have a large driving force to segregate at Al GBs. Such Mg segregation not only enhances the strength of Σ9 (221) STGB but also improves GB stability. It is found that the Mg segregation turns to enlarge and narrow the strain intervals of stable and thickening stages of Σ9 (221) STGB during tensile test, indicative of the Mg-induced stabilizing effect on the GB structural integrity. Calculations further elucidate that the segregated Mg dopants increase the critical stress for dislocation nucleation, which accounts for the remarkably increased tensile strength of Σ9 (221) STGB with Mg segregation. Such retarded dislocation nucleation is ascribed to the decrement in boundary free volume by Mg segregation. This work will provide important atomic-scale insights into the extra GB strengthening in Al alloys deriving from Mg segregation.

🙂 Springer

GRAPHICAL ABSTRACT

Mg segregation improves the strength and stability of Al grain boundary
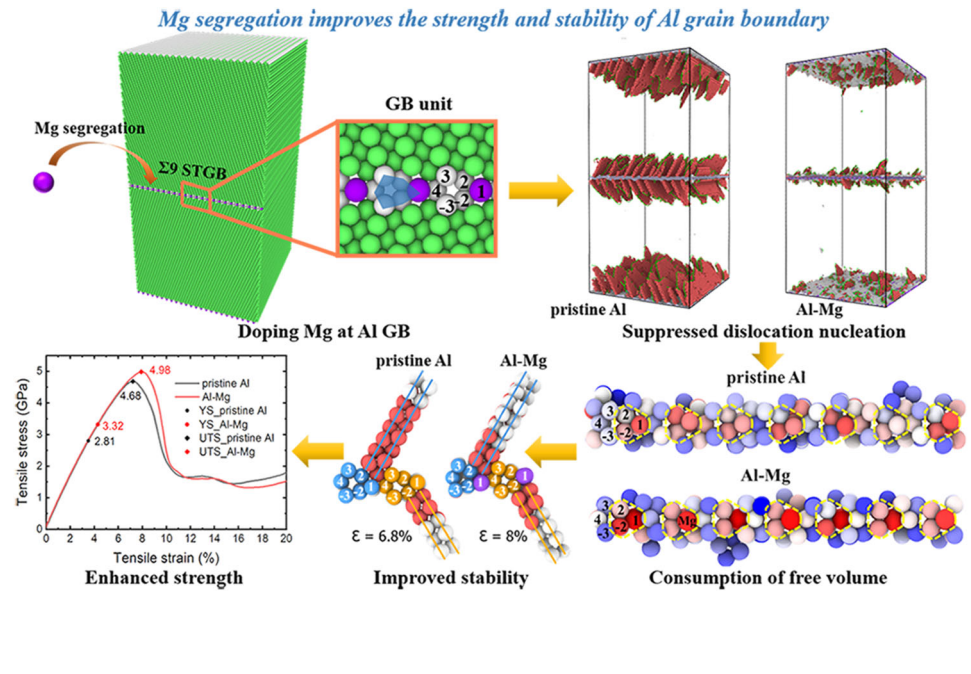
Introduction

Al alloys are widely used in various fields such as vehicle production, shipbuilding, and aerospace for energy-efficient transportation due to their light-weight and high specific strength. In recent years, bulk nanocrystalline (NC) or ultrafine-grained (UFG) Al alloys fabricated by severe plastic deformation (SPD) techniques [1–6] have gained extensive attention for their superior mechanical properties. Nevertheless, these nanostructured Al alloys usually suffer from inherent instability, especially at finite temperatures. The greatly refined grains in NC/UFG Al alloys correspond to the dramatically increased volume fraction of grain boundaries (GBs), causing a remarkable increment in the Gibbs free energy [7]. As such, grain coarsening which degrades the superior mechanical properties can be easily provoked via GB migration to alleviate the high-energy state. This accounts for the inherent instability of NC/UFG Al alloys [8].

Grain boundary segregation engineering (GBSE) [9] offers a promising pathway to improve the stability of NC/UFG materials. Generally, the alien-segregated solutes increase the GB stability in two different ways: thermodynamic and kinetic. In the thermodynamic regime, the presence of solutes at GBs will reduce GB energy, alleviating the thermodynamic driving force for GB migration [10]. As an example, Xue et al. [11, 12] found that solute doping led to a reduction in GB energy and rendered higher thermodynamic stability of the Ni GBs, while in the kinetic regime, the Zener-pinning effect by the segregated dopants is activated to suppress GB activity [13]. The strengthening due to the suppressed nucleation of partial dislocations or twins at the GBs induced by segregated solutes was observed in the Ni–B and Al–Pd alloys [14, 15]. Such restrained GB activity at the microscopic scale can notably affect the macroscopic material properties, like tensile strength, fracture toughness, corrosion resistance, etc. The stabilizing and strengthening effects owing to alien elemental doping at the GBs suggest the great potential of GBSE in optimizing the comprehensive properties of NC/UFG materials.

Following the same logic, doping of solutes at GBs has also been applied for elevating the stability and strength of NC/UFG Al alloys. As an important solute element, Mg alloying can remarkably enhance

the mechanical performances of coarse-grained Al alloys by solid solution or precipitation hardening [16, 17]. In contrast, the spatial distribution of Mg solutes in NC/UFG Al alloys differs from the coarse-grained counterparts. Except for partitioning in solid solution or precipitation, magnificent Mg segregation at GBs in these NC/UFG materials was also inspected by transmission electron microscope (TEM) [18, 19] and atom probe tomography (APT) [20–22]. Such Mg segregation is supposed to impact the microscopic GB properties and hence affect the macroscopic performances of NC/UFG Al alloys. Up to the present, multiple types of research have been dedicated to the investigation of Mg segregation and its influence on material properties. Synergistic effects of thermodynamics and kinetics in nano-scaled Al–Mg alloys with solute segregation were reported by Devaraj et al. [23], wherein the Mg segregation not only contributed to the reduction of GB energy but also facilitated the precipitation of Al_3Mg_2 which effectively pinned the GB migration. It was also demonstrated by Valiev et al. [18] that the Mg segregation at the GBs could result in extra strength exceeding the Hall–Petch predictions. The segregated Mg solutes were speculated to retard the emissions of dislocations from GBs due to the solute drag effect and reduced activation volume. The above experiments established the widely accepted extra strengthening in Al alloys deriving from GB segregation of Mg atoms. It is considered that an in-depth understanding of such segregation-induced strengthening should benefit the design and development of Al alloys with superior mechanical performances. Nevertheless, a full clarification of the underlying physics for the segregation-induced strengthening solely relying on experiments is still challenging.

Lately, atomic-scale simulations were attempted to probe the Mg segregation behavior and the resultant GB strength and stability more clearly. First-principles calculations evidenced that the doping of Mg atoms at Σ5 (210)[001] symmetric tilt grain boundary (STGB) in Al would cause GB embrittlement due to the GB expansion and charge density depletion [24, 25]. It was, however, revealed by Zhang et al. [26] that despite the weakened Al–Mg atomic bonding, the Al-Al bonding in the vicinity of Mg atoms was enhanced owing to the charge transfer, which contributes to a higher GB strength. Tensile and shear simulations using the hybrid Monte Carlo/molecular dynamics (MC/MD) method were reported by Kazemi [27, 28], wherein Mg dopants were found to inhibit GB migration under shear deformation and prevent the formation and extension of intergranular cracks, indicative of segregation-induced stabilizing effect. Despite the aforementioned experimental and computational studies on the GB segregation of Mg dopants in NC/UFG Al alloys and its effects on the GB stability and strength, the underlying physics addressing the segregation-induced stabilizing and strengthening effects, especially on the atomic level, are still less understood.

Motivated by the above considerations, MD simulations were carried out to investigate the segregation behavior of Mg atom at Al Σ9 (221)[1$\bar{1}$0] STGB and its effects on the GB stability and strength. Calculation results indicate that the structural evolution for Σ9 (221) STGBs with and without Mg segregation during uniaxial tension consists of stable, thickening, and shrinking stages, wherein the Mg segregation is shown to enlarge and narrow the strain intervals of stable and thickening stages, suggesting a stabilized GB structure after Mg segregation. Meanwhile, the segregated Mg atoms tend to retard dislocation nucleation from the GB by increasing the critical stress, accounting for the markedly enhanced yield strength after doping Mg. Structural analysis suggests that Mg segregation leads to a denser GB structure featuring decreased boundary free volume (BFV), which makes the atomic displacement/shuffling more difficult and hence suppresses dislocation nucleation from the GB.

Computational details

In Fig. 1a, bi-crystal models of NC Al with two equivalent Σ9 (221)[1$\bar{1}$0] STGBs are created, where (221) is the GB plane and [1$\bar{1}$0] refers to the tilt axis. The tilt GB was generated by rotating two single crystals along the same tilt axis [1$\bar{1}$0] in an opposite direction with a rotation angle of 19.47°. One of the two atoms was deleted from the GB models when the atomic distance between them was less than 2 Å to avoid unphysical overlapping. After constructing the pristine Al model, the Al–Mg segregation model was then built by replacing Al atoms at optimal segregation sites with Mg dopants as shown in Fig. 1b for the reason that Mg prefers to occupy substitutional sites
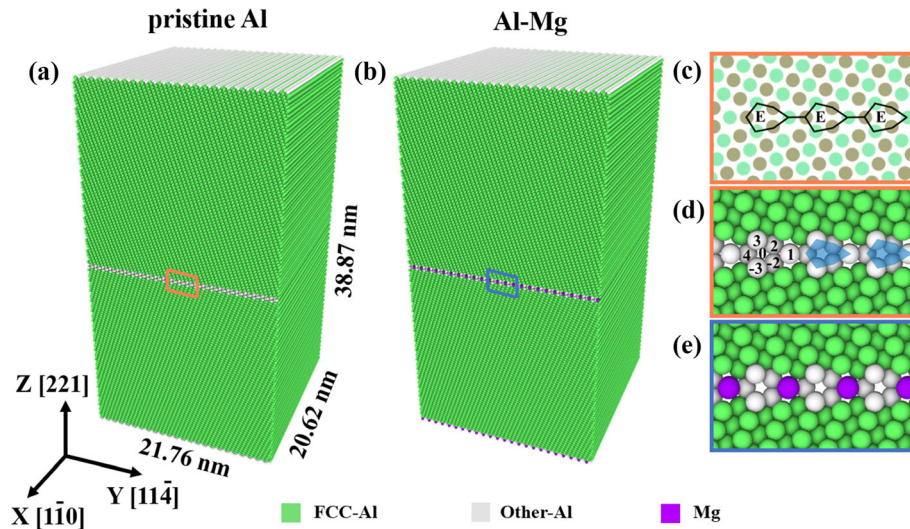
Figure 1 a The bi-crystal model of pristine Al Σ9 (221)[1$\bar{1}$0] STGB. **b** Al–Mg bi-crystal model with Mg atoms segregated at the optimal sites (Site 1). **c** Green and brown dots represent two different (1$\bar{1}$0) planes to show the atom positions in the GB. **d** GB structure of pristine Al model. E units are shown with black lines in **c** and blue polygons in **d**. Possible segregation sites of Mg are marked with numbers. **e** Al–Mg GB structure with Mg dopants segregated at Site 1. **d** and **e** are the magnified views of the rectangular area in **a** and **b**, respectively.

Table 1 The segregation energy (eV/atom) for Mg at different sites in the Σ9 (221)[1$\bar{1}$0] STGB

Segregation site	E^{GB}	E^{Bulk}	γ_{seg}
0	1.0196	0.1454	0.8742
1	− 0.0890		− 0.2344
2	0.1573		0.0119
3	− 0.0890		− 0.2344
4	0.3349		0.1895

[29]. Particularly, the optimal segregation site was determined by comparing the segregation energies of different GB sites (see Table 1 for details). Therefore, the two models have the same dimensions of simulation blocks which are 21.76 nm, 20.62 nm, and 38.87 nm in x, y, and z orientation, respectively, containing 1,046,976 atoms. As shown in Fig. 1a, the crystal orientation is [1$\bar{1}$0] in the x direction, [11$\bar{4}$] in the y direction and [221] in the z direction. In other words, the GB plane is parallel to XY plane. Note that the Miller indices involved in this article are discussed based on the coordinates of the lower grain. The periodic boundary conditions were applied in all three dimensions to avoid the free surface effect on the GB structure. Molecular statics with conjugate gradient (CG) method at a constant zero pressure was employed to carry out the following energy minimization, aiming to obtain the initial configuration with minimum energy and stable structure which were subsequently utilized for further simulation tasks.

MD simulations were performed with the open-source Large-scale Atomic/Molecular Massively Parallel Simulator (LAMMPS) package. An embedded atom method (EAM) interatomic potential in the Finnis–Sinclair type developed by Mendelev et al. [30] was employed to describe the atomic interactions in Al–Mg system, which has been regarded as the most effective potential of Al–Mg alloys so far for its ability to correctly reproduce the properties of dilute alloys of Mg in Al [31] such as solidus and liquidus in the Al-rich part of the phase diagram [30]. Uniaxial tensile tests were conducted to identify the variation of mechanical properties aroused by Mg atoms. Equilibration was carried out at the temperature of 300 K for 100 picoseconds using an isobaric-isothermal (NPT) thermostat under zero pressure to get a more stable configuration. Timestep was set to 1 fs to obtain the time integration and solve the motion equation. The tensile strain was loaded along z direction, where shrinkage and extension were allowed in both x and y directions to consider the Poisson effect. A constant strain rate of 10^{10} s^{-1} was adopted and the simulation temperature was set to

300 K during tension. Tensile strain was imposed on both samples until the total strain reached 20%.

The visualization software OVITO [32] was utilized to analyze the atomic structures and the corresponding evolution of GBs during the tensile simulations. Al atoms are colored by their local crystal structure using adaptive common neighbor analysis (CNA) implemented in OVITO, where green, red, blue, and gray represent local FCC, HCP, BCC, and unknown structures, respectively. Mg atoms are colored purple. Dislocation analysis (DXA) [33] was used to determine the structure and Burgers vector of dislocations, demonstrating the changing process of dislocation nucleation and propagation under tensile strain.

Results and discussion

Structure of $\Sigma 9$ (221)[$1\bar{1}0$] STGBs with and without Mg segregation

As shown in Fig. 1a, a bi-crystal supercell model of $\Sigma 9$ (221)[$1\bar{1}0$] pristine Al GB was constructed for tensile test, where the GB structure consists of periodic repeating arrangements of E atomic sub-structures (6-atom kite-like units marked by black lines in Fig. 1c). Such atomic structure of the $\Sigma 9$ (221) GB is well established by previous research [34–36].

From Fig. 1d, one can find that there are one interstitial segregation site (marked as Site 0) and four substitutional segregation sites in the E unit in which Site 2 and Site -2 are equivalent sites due to the symmetry of this GB. So do the Site 3 and Site -3. To construct the Al–Mg model, the segregation energy of each possible site was estimated on basis of the following equation [24]:

$$\gamma_{\text{seg}} = E^{\text{GB}} - E^{\text{Bulk}} \tag{1}$$

where E^{GB} and E^{Bulk} are the energy penalty caused by Mg doping at the Al GB and bulk, respectively. The value of E^{GB} represents the propensity of Mg atoms to dope at GBs, which can be calculated as:

$$E^{\text{GB}} = E_{\text{GB/Mg}} - E_{\text{GB}} - x \cdot \mu_{\text{Mg}} \tag{2}$$

wherein $E_{\text{GB/Mg}}$ is the energy of the bi-crystal supercell with Mg segregation, E_{GB} refers to the energy of pristine Al supercell comprising the same number of Al atoms as the segregation model, x is the number of segregated Mg atoms, and μ_{Mg} is the

chemical potential per Mg atom. E^{Bulk} indicates the tendency for Mg atoms to dope in Al matrix and is evaluated in terms of:

$$E^{\text{Bulk}} = E_{\text{Bulk/Mg}} - E_{\text{Bulk}} - x \cdot \mu_{\text{Mg}} \tag{3}$$

$E_{Bulk/Mg}$ and E_{Bulk} are the total energy of Al bulk with or without Mg dopants. As such, a negative value of γ_{seg} implies the preference for Mg solute to segregate at GB from the matrix wherein the more negative value of γ_{seg} corresponds to the higher propensity to segregate at the GB.

The values of γ_{seg} for different segregation sites are given in Table 1, which clearly shows that Site 0, Site 2, and Site 4 would not be the preferential segregation sites for Mg atoms due to the positive γ_{seg}. Specifically, after segregating at Site 0 shown in Fig. 2a, the Mg atom moved from the interstitial Site 0 to the position of the substitutional Site 1, and the original Site 1 atom is squeezed to Site 1' (cf. Figure 2b). Such segregation further led to the downward migration of the GB for a distance of h_1, resulting in local atomic rearrangement and distortion in the structural unit. This phenomenon aligns with previous studies which
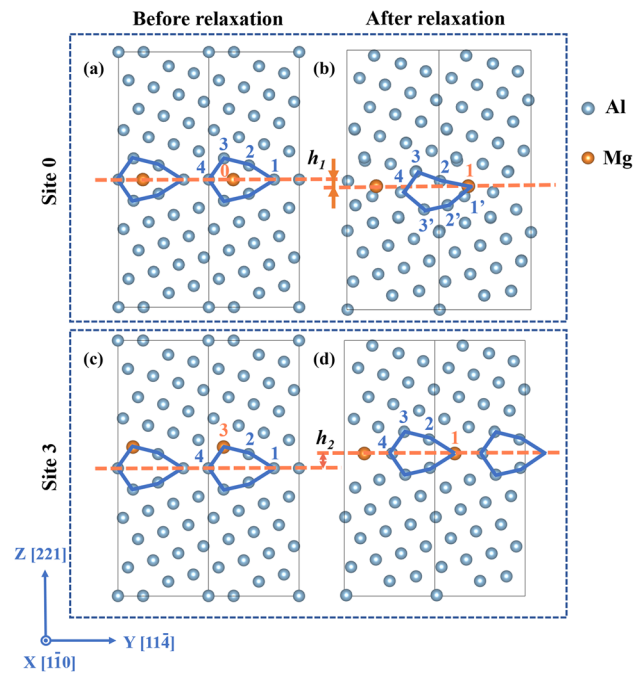

Figure 2 GB structures with Mg segregated at **a b** Site 0 and **c d** Site 3. **a c** and **b d** are structures before and after molecular static relaxation, respectively. The Al and Mg atoms are as indicated. The orange dashed lines represent the position of the GB plane. Letters h_1 and h_2 indicate the GB migration distance at Site 0 and Site 3, respectively.

demonstrate the interstitial site is not suitable for Mg segregation [24]. Additionally, it is interesting that Site 1 and Site 3 exhibit the same value γ_{seg}. To figure out the origin of this coincidence, the GB structures with Mg segregated at these two atomic sites were seriously checked. No apparent structural change was observed after adding Mg atoms to Site 1. In contrast, when Mg segregated at Site 3, the GB exhibited h_2-distance migration as marked in Fig. 2c and d and thus caused an equivalent final GB structure to that segregated at Site 1. Consequently, Site 1 is regarded as the optimal Mg segregation site in Σ9 (221) STGB with a negative γ_{seg} and stable segregation configuration. The γ_{seg} of Site 1 is − 0.234 eV/atom, which is close to − 0.279 eV/atom as previously reported on the same boundary [37]. Such a high tendency of Mg segregation to Al GBs is consistent with previous experimental and modeling results [18, 23, 24, 26–28, 38]. Further, the negative value of γ_{seg} is most likely to reduce the GB energy of Σ9 (221) GB according to the Gibbs adsorption equation, $\gamma = \gamma_0 + \Gamma_s \cdot \gamma_{seg}$, wherein γ_0 is the initial GB energy without segregation and Γ_s is the solute excess at the GB [39–41]. This implies the thermodynamic stabilization of Mg segregation on the Al GBs. As a result of the unique optimal Mg segregation at Site 1 in Σ9 (221) STGB, we build the Al–Mg segregation model shown in Fig. 1(b) by replacing all the Al atoms at Site 1 in the pristine Al GB with Mg atoms, which ends up with the monolayered Mg segregation at the GB, disclosing delta segregation feature in this work.

Uniaxial tension of Σ9 (221) GB with Mg segregation

The stress–strain curves during the uniaxial tension are plotted in Fig. 3. The critical stress for dislocation nucleation is regarded as the yield strength (YS) [42] which is 2.81 GPa for the pristine Al GB and 3.32 GPa for the Al–Mg GB with the corresponding yield strains of 3.5% and 4.25%, respectively. The ultimate tensile strength (UTS) is 4.68 GPa at 7.2% strain for the pristine Al GB and 4.98 GPa at 7.9% strain for the Al–Mg GB. Compared to pristine Al GB, the Al–Mg GB sample exhibits higher YS and UTS, indicating that the segregation of Mg atoms has strengthened the GB. Note that the Mg alloying is documented to enhance the strength of NC Al alloys via grain refinement, solid-solution strengthening, and GB
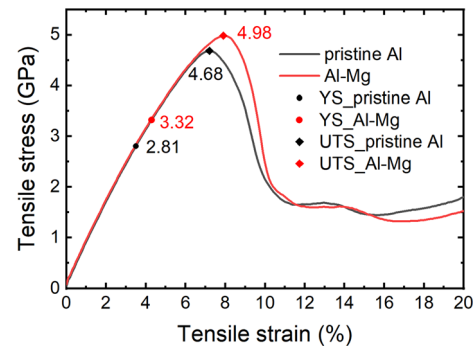

Figure 3 The stress–strain curves for the bi-crystal Σ9 (221) GB models with and without Mg segregation during uniaxial tension. The points of yield strength (YS) and ultimate tensile strength (UTS) are marked out in the curves.

segregation strengthening [18]. Considering that the two samples have the same dimensions and the Mg solutes are not introduced in the Al matrix in our work, the notably enhanced YS and UTS of the Al–Mg GB sample are completely aroused by the segregation of Mg. This behavior is in accord with the extra strengthening effect associated with Mg segregation in NC Al alloys as established by previous experimental and modeling studies [27–29, 43, 44].

The GB structures at progressive tensile strains were investigated to find out the origin of changes in the stress–strain curves of Σ9 (221) GB induced by Mg segregation. To facilitate the investigation of GB structural features, it is better to define the GB region. As shown in Fig. 4a, the area that is sandwiched by two (221) planes (blue planes) is designated as the GB region with different thicknesses of 6 Å, 8 Å, 10 Å, and 12 Å considered, wherein 6 Å is the smallest scope that could get E units contained inside the GB domain. Atoms in the GB region with different thicknesses were counted and are plotted in Fig. 4b. Note that when the tensile strain is larger than 10%, it is improper to use the counting box shown in Fig. 4a to quantify the number of GB atoms due to the severe GB distortion in the late stage of tensile deformation. Thus, only the strain ranging from 0 to 10% is discussed. One can find in Fig. 4b that when the GB thickness is 8 Å or larger, both pristine Al GB and Al–Mg GB maintain a constant number of GB atoms at 0% strain, which is around 13,600 and 12,000, respectively. As for 6 Å thickness, there is a distinct reduction in the number of GB atoms for both samples (cf. Figure 4b), suggesting that 6 Å is too thin to represent the GB domain. On the other hand, when it
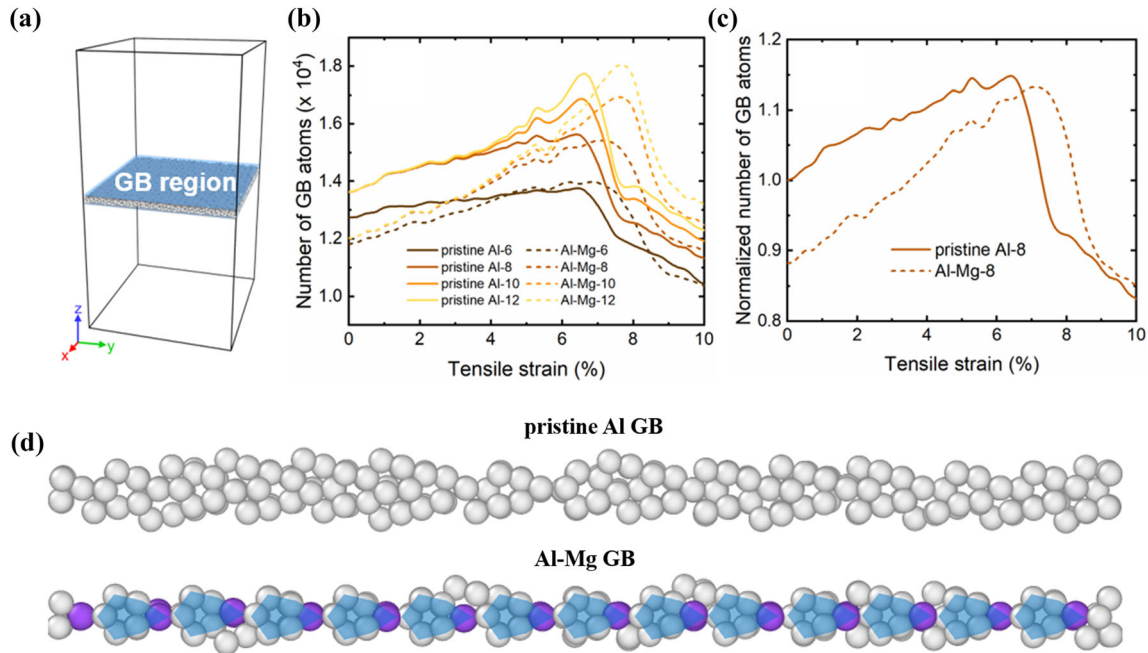
Figure 4 a The sketch of GB region defined for structural investigation. Blue planes are the (221) planes that show the borders of GB region. **b** Evolution of the number of GB atoms with GB thicknesses of 6 Å, 8 Å, 10 Å, and 12 Å till 10% strain. **c** Evolution of the normalized number of GB atoms, where 8 A was adopted as GB thickness. The number of GB atoms was normalized by the number of GB atoms in pristine Al GB model before deformation. **d** The initial GB structures for pristine Al GB and Al–Mg GB samples after equilibration, where the E units are highlighted with blue polygons.

comes to a larger thickness of 10 Å or 12 Å, extra atoms that do not belong to the GB would be counted, leading to a more pronounced maximum in the curves (cf. Figure 4b). That is to say, 10 Å or 12 Å are too thick for defining the GB domain. Moreover, the evolution of the number of GB atoms defined with 8 Å thickness is generally the same with other thicknesses at tensile strain < 4%, which justifies 8 Å as an appropriate value for the GB region.

Figure 4c displays the evolution of the normalized number of GB atoms with 8 Å thickness for both GBs. Apparently, the number of GB atoms in the Al–Mg sample is smaller than that in the pristine Al GB before tension. Such discrepancy in the numbers of GB atoms can be rationalized by the initial GB structures of both samples shown in Fig. 4d. Compared to pristine Al GB, the Al–Mg GB is more ordered with fewer extra atoms around the E units and thus contributes to the smaller number of GB atoms. It indicates that the segregated Mg atoms could enhance the initial stability of GB structure. In addition, the curves in Fig. 4c can be divided into two strain regimes. In the first regime with strain < ~ 7%, the number of GB atoms keeps increasing with

tensile strain, contributing to a thicker GB. In the second regime with strain ranging from ~ 7% to 10%, there is a rapid decline in the number of GB atoms in both models, which might be related to the shrinkage of GB. It also shows in Fig. 4c that the evolution of GB atoms of Al–Mg GB lags behind the pristine Al GB, suggesting that the Al–Mg GB has higher stability against structural distortion than pristine Al GB. This is an indication that Mg segregation would obstruct the GB structural change and hence stabilize the GB.

To gain deep insights into the changing process in the number of GB atoms caused by Mg segregation, some snapshots were captured to explore the structural evolution of pristine Al and Al–Mg GB models (cf. Figure 5). As indicated, the whole uniaxial tensile process could be divided into three stages based on the GB structural changing with increasing strain. For pristine Al GB, the first stage that is designated as the "Stable stage" corresponds to the strain of 0 ~ 3.5%, during which the E units in the GB structure were simply expanded without creating additional abnormal structural units (cf. Figure 5a). The second stage was defined as the "Thickening stage" with a strain
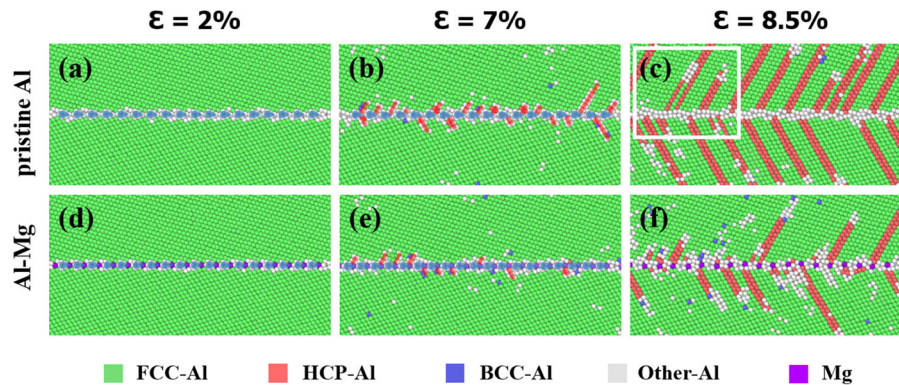
Figure 5 Snapshots of GB structural evolution for **a–c** pristine Al GB and **d–f** Al–Mg GB models during tensile simulation. **a** and **d** represent the "Stable stage"; **b** and **e** represent the "Thickening Stage"; **c** and **f** represent the "Shrinking Stage." The E units are marked with blue polygons and the irregular structural units are highlighted with red rectangles.

interval of 3.5 ~ 7.2% where the GB began to thicken and some irregular structural units marked by red rectangles started to arise (cf. Figure 5b). It is noticeable that the occurrence of these irregular structures distributing on both sides of the E units led to a more disordered boundary, which accounts for the increased number of GB atoms at tensile strain < ~ 7%. During the strain interval of 7.2 ~ 11.5%, the intrinsic stacking faults (ISFs) featured by HCP-typed atoms started to nucleate from the GB, and propagated through the grains along {111} planes, leaving behind a fish-boned structure (cf. Figure 5c). This phenomenon is also observed in Cu-Ag alloy [45]. Due to the release of ISFs, the GB thickness decreased accompanied by a greater disorder. Such decreased GB thickness explains the rapid decline in the number of GB atoms at strain ranging from ~ 7% to 10% (cf. Figure 4c). To indicate the reduction of GB thickness, this stage was designated as the "Shrinking stage." In addition, extrinsic stacking faults (ESFs) were observed in the region enclosed by the white square frame in Fig. 5c.

In comparison with pristine Al GB, the three stages characterizing the structural changes in Al–Mg GB

model took place at different tensile strains (cf. Figure 5 and Table 2). Specifically, the "Stable stage" for the Al–Mg GB model exhibits a larger strain interval than pristine Al GB, i.e., 0 ~ 5.0%. This phenomenon aligns with the ordered boundary structure found in Fig. 4d, suggesting that the stability of Σ9 (221) GB is improved by Mg segregation. Additionally, the "Thickening stage" of Al–Mg GB is postponed and contracted relative to the pristine Al GB, with a strain interval of 5 ~ 7.9%. At 7.0% strain, the number of irregular structures formed in Al–Mg GB (cf. Figure 5e) is less than that in pristine Al GB (cf. Figure 5b), where the Mg dopants are arranged in an array keeping their initial sequence unchanged. These features indicate that the segregated Mg atoms would retard the formation of irregular structures and preserve the original GB configuration. Owing to the delay of "Thickening stage," the "Shrinking stage" in Fig. 5f was also put off. However, the strain range of this stage shrank by 0.2%, which may be related to dislocation propagation and the generation of stacking faults. Compared to pristine Al GB, the extension of ISFs in Al–Mg GB seems to be blocked, which is caused by the delayed dislocation propagation with Mg doping.

Interestingly, the deformation strain of both Al and Al–Mg GBs is accommodated by ISFs and ESFs, the formation of which usually involves the nucleation of Shockley partial dislocations. As indicated in Fig. 6, a Shockley partial dislocation with Burgers vector $\frac{1}{6}[12\bar{1}]$ was emitted from the GB at 7.75% strain, causing a fault in the local stacking sequence of {111} planes, i.e., ISF. It should be noted that an ISF composed of two HCP-typed layers labeled A and C can

Table 2 The strain intervals for the three stages of GB structural evolution in the pristine Al and Al–Mg GB models during tension, including the "Stable stage," "Thickening stage," and "Shrinking stage"

	Stable stage	Thickening stage	Shrinking stage
Pristine Al	0–3.5%	3.5–7.2%	7.2–10.5%
Al–Mg	0–5%	5–7.9%	7.9–11%

Figure 6 a–c Snapshots showing the formation of ISFs and ESFs within the white box area in Fig. 5e. **a** A Shockley partial dislocation marked by a circle was connected with ISF at 7.75% strain. **b** Another Shockley partial dislocation nucleated from GB on the adjacent {111} slip plane at 8.25% strain. **c** Formation of ESF via successive nucleation of partial dislocations. A B and C refer to different atomic layers, which indicate the stacking sequence. **d–f** Snapshots showing the structures of ISFs, ESFs, and twins in the pristine Al GB. FCC-typed atoms were deleted to show the inner structures.
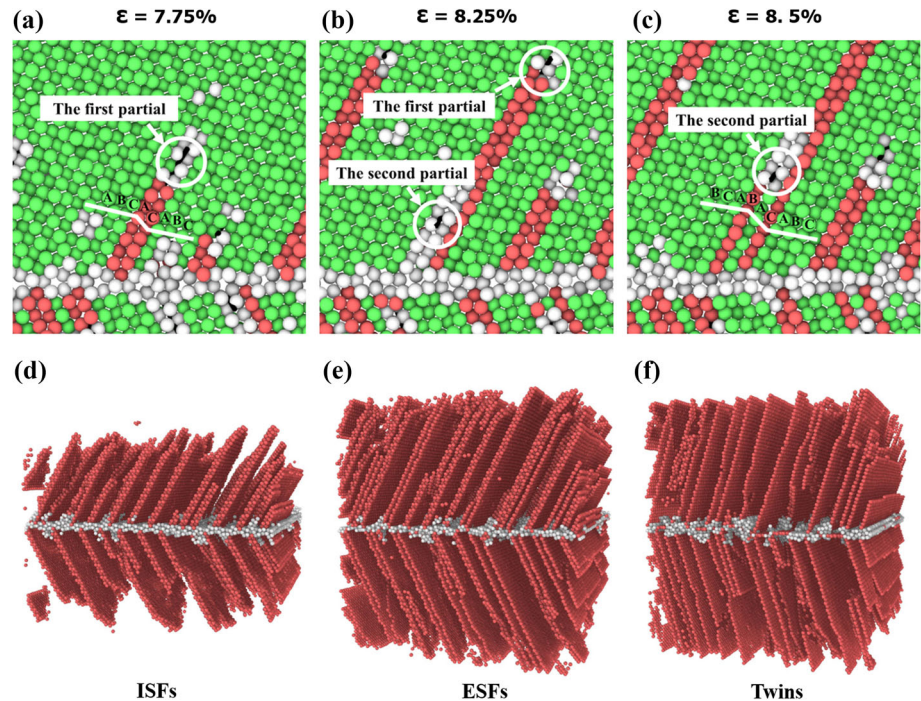
be regarded as the result of removing one B-type layer from the perfect stacking sequence ABC. At the strain of 8.25%, the nucleation of a second Shockley partial dislocation with the same Burgers vector on the adjacent {111} sliding plane was observed, leading to the formation of a two-layer microtwin, which is also designated as the ESF with a stacking sequence of BAC (cf. Figure 6c). With the successive nucleation of partial dislocations, the two-layer micro-twins would eventually grow into larger twins (cf. Figure 6d–f).

This observation has been widely verified by experiments [46–48]. On basis of generalized stacking fault energy, Frøseth et al. [49] and Zhao et al. [50] documented that there are three possible deformation mechanisms for FCC metals, i.e., extended stacking faults, full dislocations, and deformation twinning, wherein the full dislocation slip was believed to be dominant in coarse-grained Al when subjected to plastic deformation. However, no full dislocation is detected in the pristine Al and Al–Mg GB models during uniaxial tensile simulations. Only nucleation of Shockley partial from the GB and its absorption by the opposite GB was observed, leaving the grain transected by ISFs and ESFs. The absence of full dislocation behavior in this simulation is likely ascribed to the fact that the splitting distance of extended dislocation is probably larger than the grain

size/thickness as adopted in this work. This would notably restrict the subsequent emission of trailing Shockley partial to form a full dislocation, thus making the Shockley partials and extended stacking faults the dominant deformation behaviors in the present simulation [51].

Effect of Mg segregation on partial dislocation behavior

Further analysis of the partial dislocation behaviors was carried out to gain deep insights into the enhanced GB strength induced by Mg segregation. Figure 7 shows the dislocation nucleation process in pristine Al and Al–Mg GB models. As indicated in Fig. 7a, the partial dislocation labeled A started to nucleate at 3.5% strain. But it subsequently disappeared at the strain of 3.75% (cf. Figure 7b). It is noteworthy that this phenomenon is not special for partial A. Actually, all the dislocations would experience this "nucleate-disappear" procedure in the starting stage of tensile deformation, which is designated as the "unstable nucleation period" for dislocations. The significant growth of dislocation B observed in Fig. 7c and d marks the end of this period, where B could exist stably instead of vanishing after nucleation. The stable nucleation strain is thus determined to be 6%, smaller than the critical strain
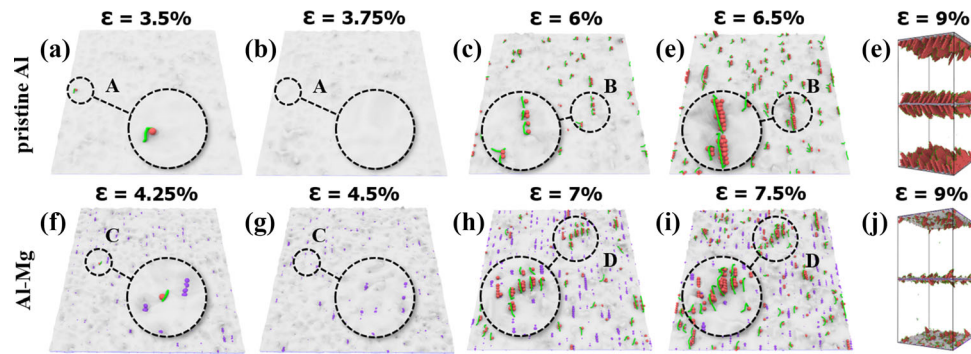
Figure 7 Snapshots showing the partial dislocation behaviors in **a–e** pristine Al and **f–j** Al–Mg GB models during tensile deformation. The light gray plane represents the GB. Shockley partial dislocations are labeled with green lines. Letters A, B, C, and D indicate the dislocations observed at different strains. **e** and **j** display the 3-D morphologies of dislocations at 9% strain in both models, wherein only the HCP-type atoms are shown.

of 7.2% in the stress–strain curve, above which the strength starts to decrease (cf. Figure 3). Similar results have been reported on Σ11 tilt GBs in copper bicrystals wherein the stress–strain curve does not drop immediately after dislocation nucleation [52].

Figure 8 records the evolution of dislocation number at the starting stage where the fluctuation shown in the insets further confirms the existence of the unstable period. By comparing the dislocation behaviors in Fig. 7 and the evolution of dislocation number in Fig. 8, the strain range for the unstable nucleation period for pristine Al GB is determined to be 3.5% ∼ 6% (cf. Table 3). As for Al–Mg GB sample, similar structural degeneration of dislocations was also observed, as indicated by the emergence and disappearance of partial C in Fig. 7f and g at the strains of ∼ 4.25% and ∼ 4.5%, respectively. It is seen from Fig. 7h–i that the stable dislocation emission from Al–Mg GBs occurred at ∼ 7% strain, where dislocations marked with D propagate progressively instead of vanishing. Comparing the strain intervals of unstable nucleation

Table 3 The strain intervals of unstable nucleation period in the pristine Al and Al–Mg GB models during uniaxial tensions

	Pristine Al (%)	Al–Mg (%)
Initial dislocation nucleation	3.5	4.25
Stable dislocation nucleation	6	7
Interval of unstable period	2.5	2.75

period of pristine Al and Al–Mg GB models (cf. Table 3 and Fig. 8), one can apparently find that with segregated Mg the strain for first dislocation nucleation is delayed by 0.75% and the strain interval of unstable nucleation period is prolonged by 0.25%. Such delayed nucleation of GB dislocations and enlarged unstable nucleation period suggest the retarding effect of Mg segregation on GB dislocation nucleation, which contributes to the larger yield strength of Al–Mg GB than pristine Al GB model. The suppressed dislocation nucleation is better displayed with the three-dimensional morphologies in Fig. 7e and j, wherein the Al–Mg GB model contains much

Figure 8 Evolution of the number of nucleated dislocations in **a** pristine Al and **b** Al–Mg GB samples during tensile tests before the onset of plastic flow. The insets show the fluctuations of nucleated dislocation numbers at the starting stage of deformation in both samples.
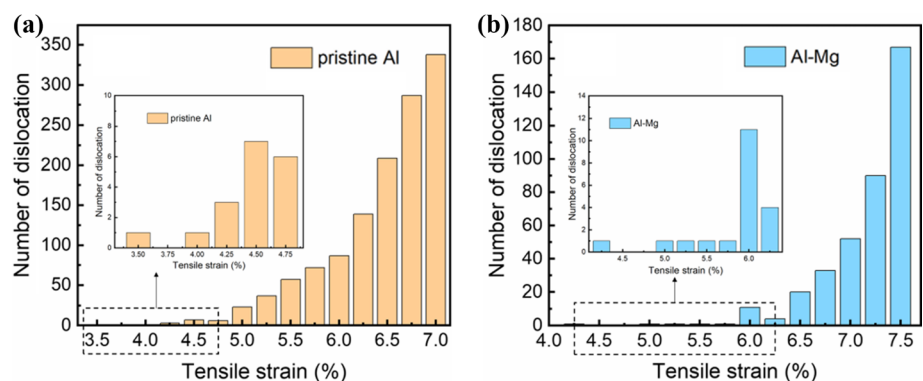
fewer nucleated dislocations than pristine Al GB at the same strain. Such restrained dislocation motion has been reported on Cu-Ag alloy where the segregated solutes at the GB act as obstacles to dislocation nucleation [45].

In order to reveal the atomic mechanism for dislocation nucleation, the migration of atoms occurring at the GB was investigated. Figure 9a–d shows the displacement vectors of GB atoms, which measure the atomic migration from their initial positions to current positions. As indicated in Fig. 9a and b, during the unstable nucleation period, individual GB atoms move rather disorderly with small displacements in local domains. Instantaneous atomic aggregation occurs at certain positions, the atomic displacement of which accidentally satisfies the Burgers vector requirement to nucleate partials and hence forms a small dislocation core. The disordered atomic migration at small strains makes such nucleated dislocations unstable and unable to propagate into the grain interior. Moreover, the shuffling of aggregated atoms at increased tensile strains will result in the disappearance of the nucleated dislocation structure. As such, structural fluctuation in terms of iterative formation and disappearance of

dislocation cores can frequently occur at the GB, and this leads to unstable dislocation nucleation at early tensile deformation. When the strain increases to a critical value, the GB atoms start to undergo large-scale coordinated migration as shown in Fig. 9c–d. The pronounced collective atomic migration can afford the progressive nucleation and propagation of dislocations from the GBs, which accounts for the stable dislocation nucleation at relatively larger strains. Immediately after dislocation nucleation, collective migration of GB atoms from the non-nucleation area to the region where dislocations nucleate can be apparently observed (cf. Figure 9c–d). Similar collective atomic migration behavior after dislocation nucleation was also reported by Tucker et al. [53]. Notably, atoms on the right side of nucleation region have much smaller displacements than that on the left side. It is the different displacements on both sides of the nucleation region that leads to the stable emission of dislocations from the GB.

The aforementioned GB activation event for partials in terms of atomic rearrangement and migration is strongly governed by the atomic free volume at the GB [18, 54–57]. Hence, quantifying the free volume of GB atoms helps to elucidate the effects of Mg
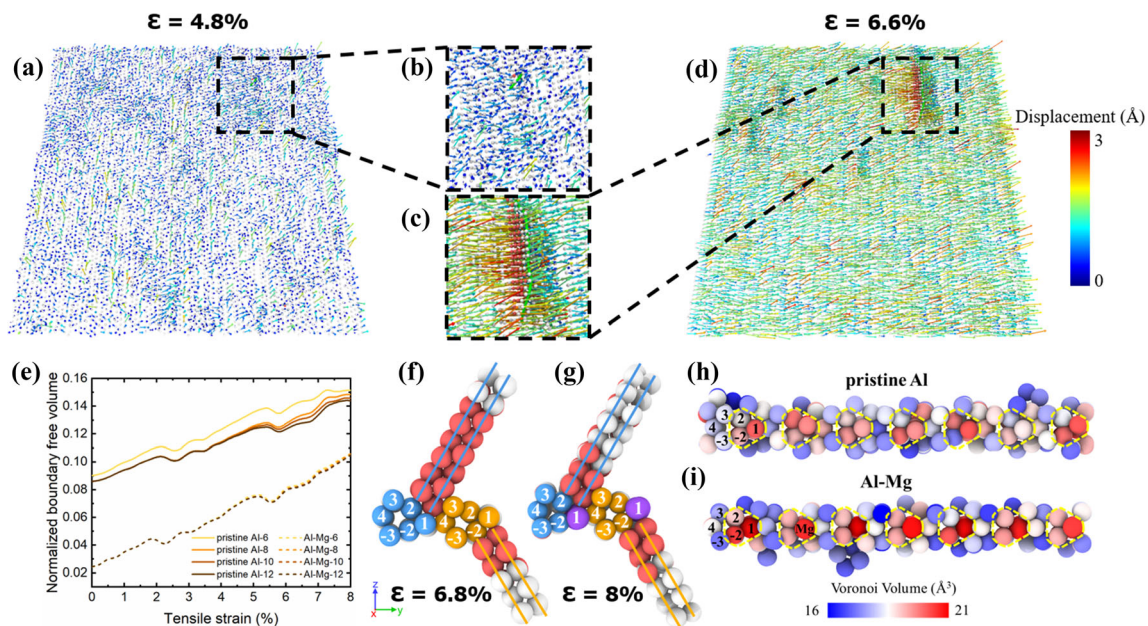

Figure 9 The distribution of atomic displacement in pristine Al GBs **a** during and **d** after unstable nucleation period. **b** and **c** are the enlarged views of dashed squares in **a** and **d**. **e** Normalized boundary free volume versus tensile strain in both models. GB domain with thicknesses of 6 Å, 8 Å, 10 Å, and 12 Å was computed. **f** and **g** are the snapshots of ISFs emitted from E units in pristine Al and Al–Mg GBs, respectively. **h** and **i** are the Voronoi volume distribution of GB atoms at 3.5% strain in both models, where the area with a large volume is marked by the yellow dashed line.

segregation on the atomic displacements and dislocation nucleation at the GB. BFV is widely used to indicate the sparseness of GBs relative to the matrix. For the pristine Al GB model, the BFV can be predicted by [58]:

$$\mathrm{BFV}_{(Al-GB)} = \frac{v_{Al}^{GB} - v_{Al}^{Bulk}}{v_{Al}^{Bulk}} \tag{4}$$

where v_{Al}^{GB}, v_{Al}^{Bulk} are the average atomic volume of Al atoms in the GB area or perfect *fcc* crystals. While for binary or higher-order systems, Eq. (4) should be revised to eliminate the influence aroused by the radius difference between solute dopants and host atoms. As for the Al–Mg GB model, the BFV can be evaluated as [55]:

$$\mathrm{BFV}_{(Al-Mg)} = \frac{V_{Al-Mg}^{GB} - N_{Al} \cdot v_{Al}^{Bulk} - N_{Mg} \cdot v_{Mg}^{Bulk}}{N_{Al} \cdot v_{Al}^{Bulk} + N_{Mg} \cdot v_{Mg}^{Bulk}} \tag{5}$$

where v_{Mg}^{GB}, v_{Mg}^{Bulk} are the average atomic volume of Mg atoms in the GB area or perfect *hcp* crystals. N_{Al} and N_{Mg} refer to the numbers of Al and Mg atoms in the GB domain, while V_{Al-Mg}^{GB} is the total volume of GB region in the Al–Mg GB model, which can be computed with the following:

$$V_{Al-Mg}^{GB} = N_{Al} \cdot v_{Al}^{GB} + N_{Mg} \cdot v_{Mg}^{GB} \tag{6}$$

Herein, all the atomic volume was obtained by calculating the Voronoi volume with OVITO. It is noteworthy that Eqs. (4) and (5) are essentially equivalent and both of them provide a normalized approach for computing BFV, which facilitates the direct BFV comparison in different systems.

Figure 9e displays the normalized BFV versus tensile strain for both GBs, which were evaluated with different GB thicknesses. It is conspicuously seen that the BFV of both models ascends with tensile strain up to 8%. One can find the Al–Mg model exhibits almost the same evolution of BFV for different GB thicknesses, while for pristine Al GB model, the calculated BFV of 6 Å thickness is remarkably larger than the other three thicknesses. Consequently, 8 Å is further proved appropriate for defining the GB domain. Moreover, the Al–Mg sample shows a significant reduction in BFV as compared with pristine Al sample throughout the tensile deformation. Such reduction in BFV inhibits the GB atomic reordering and thus suppresses the relative displacement between adjacent slip planes which is necessary for dislocation nucleation. When the Mg atoms segregate at GB and lead to a smaller BFV, the dislocation nucleation is suppressed due to the restricted relative displacement. Partials become more difficult to nucleate; thus, larger critical stress is needed. The inverse dependence between BFV and yield stress found in the present work is analogous to previous research on other alloy systems [42, 54, 55, 59], wherein the decline in free volume provoked by the presence of alien elemental doping turns to suppress the dislocation nucleation/emission from the GBs. Previous research also testifies that Mg segregation can weaken the chemical bonding of Al GBs due to GB expansion and charge density depletion [24]. Despite the weakening effect, it seems not decisive when referring to the GB strength controlled by dislocation activities.

It can be further seen from Fig. 9f–g that the ISFs (marked with blue and orange lines) are mostly emitted from Site 1 and Site 2 (or Site -2) of the E unit. The preferential nucleation of partials at specific GB core sites is supposed to be related to the heterogeneous distribution of free volume at the GB. The Voronoi volume of GB atoms was hence colorized to visualize the free volume distribution. As shown in Fig. 9h, Site 1 and Site 2 (or Site -2) in pristine Al GB occupy notably higher free volume than the others, indicating that these sites are more prone to migrate under applied tensile stress, leading to local atomic rearrangement and free volume migration as well as the nucleation of partial dislocations and the formation of ISFs. However, the segregated Mg atoms alter the atomic volume distribution of $\Sigma 9$ (221) GB (cf. Figure 9i). Specifically, the average atomic volume of Al atoms in the GB region of pristine Al and Al–Mg models is 18.03 $\mathrm{\AA}^3$ and 17.69 $\mathrm{\AA}^3$, respectively. It means that the spacing between Al atoms is reduced and the GB structure becomes more compact after Mg segregation. On the other hand, the distance between Al and Mg atoms increases, leading to GB expansion. Since the ratio of Al atoms to Mg atoms is close to 5:1 per unit, the contractive effect is dominant, contributing to the decline in BFV. The atomic volume distribution in both GB models elucidates why solutes with a larger size than host atoms would lead to a decrease in BFV of the Al–Mg GB. It is noteworthy that the evolution of free volume is strictly coupled with atomic migration/displacement at the GB, wherein free volume normally migrates in the opposite direction of atomic displacement. A

denser GB structure with Mg occupying a part of the atomic free volume of GB core sites will result in the decreased mobility of atoms and suppressed migration of free volume, thereby inhibiting the nucleation of dislocations. As a result, the critical stress for dislocation nucleation is considerably increased, which accounts for the delay in dislocation nucleation observed in Fig. 7 and the increment in yield strength shown in Fig. 3.

Conclusion

The Mg segregation at $\Sigma 9$ (221)[$1\bar{1}0$] STGB in Al and its effects on GB stability and strength were systematically studied via molecular dynamics simulations for understanding the extra strengthening induced by GB segregation of Mg solutes. From our simulation, several important conclusions are obtained as follows:

- Consistent with experiments, the calculation results suggest that alien Mg impurity shows a large propensity to segregate at $\Sigma 9$ (221) STGB in Al. Such Mg segregation turns to decrease the GB energy, implicating a thermodynamic stabilization.
- The preferential Mg segregation notably enhances the strength of $\Sigma 9$ (221) STGB, wherein an increment of ~ 500 MPa in the yield strength and ~ 300 MPa in the ultimate tensile strength during tensile deformation was observed.
- The GB structural evolution for $\Sigma 9$ (221) STGBs with and without Mg segregation during tensile deformation consists of three typical stages, i.e., stable, thickening, and shrinking stages. The Mg segregation is revealed to enlarge and narrow the strain intervals of stable and thickening stages, suggesting the stabilized GB structure with Mg segregation.
- The segregated Mg dopants were demonstrated to retard dislocation nucleation by increasing the critical stress, which leads to the notably increased tensile strength of $\Sigma 9$ (221) STGB after doping Mg.
- The denser GB structure with segregated Mg featuring decreased BFV makes the atomic displacement/shuffling and free volume migration more difficult and hence is considered responsible for the retarded dislocation nucleation from the GBs.

Declarations

Conflict of interest The authors declare that they have no conflict of interest.

References

[1] Jia H, Bjørge R, Cao L, Song H, Marthinsen K, Li Y (2018) Quantifying the grain boundary segregation strengthening induced by post-ECAP aging in an Al-5Cu alloy. Acta Mater 155:199–213. https://doi.org/10.1016/j.actamat.2018.05.075

[2] Zha M, Li Y, Mathiesen RH, Bjørge R, Roven HJ (2015) Microstructure evolution and mechanical behavior of a binary Al-7Mg alloy processed by equal-channel angular pressing. Acta Mater 84:42–54. https://doi.org/10.1016/j.actamat.2014.10.025

[3] Zha M, Zhang H, Jia H, Gao Y, Jin S, Sha G, Bjørge R, Mathiesen RH, Roven HJ, Wang H, Li Y (2021) Prominent role of multi-scale microstructural heterogeneities on superplastic deformation of a high solid solution Al-7Mg alloy. Int J Plast 146:103108. https://doi.org/10.1016/j.ijplas.2021.103108

[4] Sauvage X, Duchaussoy A, Zaher G (2019) Strain induced segregations in severely deformed materials. Mater Trans 60(7):1151–1158. https://doi.org/10.2320/matertrans.MF201919

[5] Swaminathan S, Ravi Shankar M, Rao BC, Compton WD, Chandrasekar S, King AH, Trumble KP (2007) Severe plastic deformation (SPD) and nanostructured materials by machining. J Mater Sci 42(5):1529–1541. https://doi.org/10.1007/s10853-006-0745-9

[6] Valiev RZ, Islamgaliev RK, Alexandrov IV (2000) Bulk nanostructured materials from severe plastic deformation. Prog Mater Sci 45(2):103–189. https://doi.org/10.1016/S0079-6425(99)00007-9

[7] Chookajorn T, Murdoch HA, Schuh CA (2012) Design of stable nanocrystalline alloys. Science 337:951–954. https://doi.org/10.1126/science.1224737

[8] Sauvage X, Murashkin MY, Straumal BB, Bobruk EV, Valiev RZ (2015) Ultrafine grained structures resulting from SPD-induced phase transformation in Al-Zn alloys. Adv Eng Mater 17(12):1821–1827. https://doi.org/10.1002/adem.201500151

[9] Raabe D, Herbig M, Sandlöbes S, Li Y, Tytko D, Kuzmina M, Ponge D, Choi PP (2014) Grain boundary segregation engineering in metallic alloys: a pathway to the design of interfaces. Curr Opin Solid State Mater Sci 18(4):253–261. https://doi.org/10.1016/j.cossms.2014.06.002

[10] Koch CC, Scattergood RO, Darling KA, Semones JE (2008) Stabilization of nanocrystalline grain sizes by solute additions. J Mater Sci 43(23–24):7264–7272. https://doi.org/10.1007/s10853-008-2870-0

[11] Xue H, Luo Y, Tang F, Yu X, Lu X, Ren J (2021) Solute segregation induced stabilizing and strengthening effects on Ni Σ3 [110](111) symmetrical tilt grain boundary in nickel-based superalloys. J Mater Res Technol 11:1281–1289. https://doi.org/10.1016/j.jmrt.2021.01.066

[12] Xue H, Luo Y, Tang F, Lu X, Ren J (2021) Segregation behavior of alloying elements at Ni Σ5 [001](210) symmetrical tilt grain boundary in nickel-based superalloys and their stabilization and strengthening mechanisms for the grain boundary. Mater Chem Phys 258:123977. https://doi.org/10.1016/j.matchemphys.2020.123977

[13] Lu K (2016) Stabilizing nanostructures in metals using grain and twin boundary architectures. Nat Rev Mater 1(5):16019. https://doi.org/10.1038/natrevmats.2016.19

[14] Tytko D, Choi P-P, Klöwer J, Kostka A, Inden G, Raabe D (2012) Microstructural evolution of a Ni-based superalloy (617B) at 700°C studied by electron microscopy and atom probe tomography. Acta Mater 60(4):1731–1740. https://doi.org/10.1016/j.actamat.2011.11.020

[15] Jang S, Purohit Y, Irving DL, Padgett C, Brenner D, Scattergood RO (2008) Influence of Pb segregation on the deformation of nanocrystalline Al: Insights from molecular simulations. Acta Mater 56(17):4750–4761. https://doi.org/10.1016/j.actamat.2008.05.024

[16] Schoenitz M, Dreizin E (2003) Structure and properties of Al–Mg mechanical alloys. J Mater Res 18:1827–1836. https://doi.org/10.1557/JMR.2003.0255

[17] Król M, Tański T, Snopiński P, Tomiczek B (2016) Structure and properties of aluminium-magnesium casting alloys after heat treatment. J Therm Anal Calorim 127(1):299–308. https://doi.org/10.1007/s10973-016-5845-4

[18] Valiev RZ, Enikeev NA, Murashkin MY, Kazykhanov VU, Sauvage X (2010) On the origin of the extremely high strength of ultrafine-grained Al alloys produced by severe plastic deformation. Scr Mater 63(9):949–952. https://doi.org/10.1016/j.scriptamat.2010.07.014

[19] Malls T, Chaturvedi MC (1982) Grain-boundary segregation in an Al-8 wt % Mg alloy. J Mater Sci 17:1479–1486. https://doi.org/10.1007/BF00752263

[20] Masuda T, Sauvage X, Hirosawa S, Horita Z (2020) Achieving highly strengthened Al-Cu-Mg alloy by grain refinement and grain boundary segregation. Mater Sci Eng A 793:139668. https://doi.org/10.1016/j.msea.2020.139668

[21] Sha G, Yao L, Liao X, Ringer SP, Chao Duan Z, Langdon TG (2011) Segregation of solute elements at grain boundaries in an ultrafine grained Al-Zn-Mg-Cu alloy. Ultramicroscopy 111(6):500–505. https://doi.org/10.1016/j.ultramic.2010.11.013

[22] Liddicoat PV, Liao XZ, Zhao Y, Zhu Y, Murashkin MY, Lavernia EJ, Valiev RZ, Ringer SP (2010) Nanostructural hierarchy increases the strength of aluminium alloys. Nat Commun 1:63. https://doi.org/10.1038/ncomms1062

[23] Devaraj A, Wang W, Vemuri R, Kovarik L, Jiang X, Bowden M, Trelewicz JR, Mathaudhu S, Rohatgi A (2019) Grain boundary segregation and intermetallic precipitation in coarsening resistant nanocrystalline aluminum alloys. Acta Mater 165:698–708. https://doi.org/10.1016/j.actamat.2018.09.038

[24] Zhao D, Løvvik OM, Marthinsen K, Li Y (2018) Segregation of Mg, Cu and their effects on the strength of Al Σ5 (210)[001] symmetrical tilt grain boundary. Acta Mater 145:235–246. https://doi.org/10.1016/j.actamat.2017.12.023

[25] Hu J, Xiao Z, Huang Y (2021) Segregation of solute elements and their effects on the strength of Al Σ5 (210) [001] symmetrical tilt grain boundary in 2219 alloys. Mater Sci Eng A 800:140261. https://doi.org/10.1016/j.msea.2020.140261

[26] Zhang S, Kontsevoi OY, Freeman AJ, Olson GB (2012) Cohesion enhancing effect of magnesium in aluminum grain boundary: A first-principles determination. Appl Phys Lett 100(23):231904. https://doi.org/10.1063/1.4725512

[27] Kazemi A, Yang S (2019) Atomistic study of the effect of magnesium dopants on the strength of nanocrystalline aluminum. JOM 71(4):1209–1214. https://doi.org/10.1007/s11837-019-03373-3

[28] Kazemi A, Yang S (2021) Effects of magnesium dopants on grain boundary migration in aluminum-magnesium alloys. Comput Mater Sci 188:110130. https://doi.org/10.1016/j.commatsci.2020.110130

[29] Lee B-H, Kim S-H, Park J-H, Kim H-W, Lee J-C (2016) Role of Mg in simultaneously improving the strength and ductility of Al-Mg alloys. Mater Sci Eng A 657:115–122. https://doi.org/10.1016/j.msea.2016.01.089

[30] Mendelev MI, Asta M, Rahman MJ, Hoyt JJ (2009) Development of interatomic potentials appropriate for simulation of solid-liquid interface properties in Al-Mg alloys. Philos Mag 89(34–36):3269–3285. https://doi.org/10.1080/14786430903260727

[31] Jelinek B, Houze J, Kim S, Horstemeyer MF, Baskes MI, Kim S-G (2007) Modified embedded-atom method

interatomic potentials for the Mg-Al alloy system. Phys Rev B 75(5):054106. https://doi.org/10.1103/PhysRevB.75.054106

[32] Stukowski A (2010) Visualization and analysis of atomistic simulation data with OVITO–the open visualization tool. Modell Simul Mater Sci Eng 18(1):015012. https://doi.org/10.1088/0965-0393/18/1/015012

[33] Stukowski A, Bulatov VV, Arsenlis A (2012) Automated identification and indexing of dislocations in crystal interfaces. Modell Simul Mater Sci Eng 20(8):085007. https://doi.org/10.1088/0965-0393/20/8/085007

[34] Shen XJ, Tanguy D, Connétable D (2014) Atomistic modelling of hydrogen segregation to the $\Sigma 9$ 221 [110] symmetric tilt grain boundary in Al. Philos Mag 94(20):2247–2261. https://doi.org/10.1080/14786435.2014.910333

[35] Wan L, Wang S (2010) Shear response of the $\Sigma 9$ <110> {221} symmetric tilt grain boundary in fcc metals studied by atomistic simulation methods. Phys Rev B 82(21):214112. https://doi.org/10.1103/PhysRevB.82.214112

[36] Hardouinduparc O, Couzinie J, Thibaultpenisson J, Lartiguekorinek S, Decamps B, Priester L (2007) Atomic structures of symmetrical and asymmetrical facets in a near $\Sigma=9${221} tilt grain boundary in copper. Acta Mater 55(5):1791–1800. https://doi.org/10.1016/j.actamat.2006.10.041

[37] Mahjoub R, Laws KJ, Stanford N, Ferry M (2018) General trends between solute segregation tendency and grain boundary character in aluminium—an ab initio study. Acta Mater 158:257–268. https://doi.org/10.1016/j.actamat.2018.07.069

[38] Babicheva RI, Dmitriev SV, Bai L, Zhang Y, Kok SW, Kang G, Zhou K (2016) Effect of grain boundary segregation on the deformation mechanisms and mechanical properties of nanocrystalline binary aluminum alloys. Comput Mater Sci 117:445–454. https://doi.org/10.1016/j.commatsci.2016.02.013

[39] Saber M, Kotan H, Koch CC, Scattergood RO (2013) Thermodynamic stabilization of nanocrystalline binary alloys. J Appl Phys 113(6):063515. https://doi.org/10.1063/1.4791704

[40] Liu F, Kirchheim R (2004) Nano-scale grain growth inhibited by reducing grain boundary energy through solute segregation. J Cryst Growth 264(1–3):385–391. https://doi.org/10.1016/j.jcrysgro.2003.12.021

[41] Lejček P, Šob M, Paidar V (2017) Interfacial segregation and grain boundary embrittlement: an overview and critical assessment of experimental data and calculated results. Prog Mater Sci 87:83–139. https://doi.org/10.1016/j.pmatsci.2016.11.001

[42] Turlo V, Rupert TJ (2018) Grain boundary complexions and the strength of nanocrystalline metals: dislocation emission and propagation. Acta Mater 151:100–111. https://doi.org/10.1016/j.actamat.2018.03.055

[43] Pun SC, Wang W, Khalajhedayati A, Schuler JD, Trelewicz JR, Rupert TJ (2017) Nanocrystalline Al-Mg with extreme strength due to grain boundary doping. Mater Sci Eng A 696:400–406. https://doi.org/10.1016/j.msea.2017.04.095

[44] Rahman MJ, Zurob HS, Hoyt JJ (2016) Molecular dynamics study of solute pinning effects on grain boundary migration in the aluminum magnesium alloy system. Metall Mater Trans A 47(4):1889–1897. https://doi.org/10.1007/s11661-016-3322-0

[45] Borovikov V, Mendelev MI, King AH (2017) Effects of solutes on dislocation nucleation from grain boundaries. Int J Plast 90:146–155. https://doi.org/10.1016/j.ijplas.2016.12.009

[46] Liao XZ, Zhou F, Lavernia EJ, He DW, Zhu YT (2003) Deformation twins in nanocrystalline Al. Appl Phys Lett 83(24):5062–5064. https://doi.org/10.1063/1.1633975

[47] Chen M, Ma E, Hemker KJ, Sheng H, Wang Y, Cheng X (2003) Deformation twinning in nanocrystalline aluminum. Science 300(5623):1275–1277. https://doi.org/10.1126/science.1083727

[48] Zhu YT, Liao XZ, Wu XL (2012) Deformation twinning in nanocrystalline materials. Prog Mater Sci 57(1):1–62. https://doi.org/10.1016/j.pmatsci.2011.05.001

[49] Frøseth AG, Derlet PM, Van Swygenhoven H (2005) Twinning in nanocrystalline fcc metals. Adv Eng Mater 7(1–2):16–20. https://doi.org/10.1002/adem.200400163

[50] Zhao D, Løvvik OM, Marthinsen K, Li Y (2016) Impurity effect of Mg on the generalized planar fault energy of Al. J Mater Sci 51(14):6552–6568. https://doi.org/10.1007/s10853-016-9834-6

[51] Yamakov V, Wolf D, Salazar M, Phillpot SR, Gleiter H (2001) Length-scale effects in the nucleation of extended dislocations in nanocrystalline Al by molecular-dynamics simulation. Acta Mater 49:2713–2722. https://doi.org/10.1016/S1359-6454(01)00167-7

[52] Zhang L, Lu C, Tieu K, Zhao X, Pei L (2015) The shear response of copper bicrystals with Sigma11 symmetric and asymmetric tilt grain boundaries by molecular dynamics simulation. Nanoscale 7(16):7224–7233. https://doi.org/10.1039/c4nr07496c

[53] Tucker GJ, Tschopp MA, McDowell DL (2010) Evolution of structure and free volume in symmetric tilt grain boundaries during dislocation nucleation. Acta Mater 58(19):6464–6473. https://doi.org/10.1016/j.actamat.2010.08.008

[54] Vo NQ, Schäfer J, Averback RS, Albe K, Ashkenazy Y, Bellon P (2011) Reaching theoretical strengths in nanocrystalline Cu by grain boundary doping. Scr Mater 65(8):660–663. https://doi.org/10.1016/j.scriptamat.2011.06.048

[55] Li A, Szlufarska I (2017) Morphology and mechanical properties of nanocrystalline Cu/Ag alloy. J Mater Sci 52(8):4555–4567. https://doi.org/10.1007/s10853-016-0700-3

[56] Uesugi T, Higashi K (2011) First-principles calculation of grain boundary energy and grain boundary excess free volume in aluminum: role of grain boundary elastic energy. J Mater Sci 46(12):4199–4205. https://doi.org/10.1007/s10853-011-5305-2

[57] Huang Z, Chen F, Shen Q, Zhang L, Rupert TJ (2019) Combined effects of nonmetallic impurities and planned metallic dopants on grain boundary energy and strength. Acta Mater 166:113–125. https://doi.org/10.1016/j.actamat.2018.12.031

[58] Sun H, Singh CV (2020) Temperature dependence of grain boundary excess free volume. Scr Mater 178:71–76. https://doi.org/10.1016/j.scriptamat.2019.10.046

[59] Chang KI, Hong SI (2008) Effect of sulphur on the strengthening of a Zr–Nb alloy. J Nucl Mater 373(1–3):16–21. https://doi.org/10.1016/j.jnucmat.2007.04.045